RSC Advances

REVIEW

View Article Online
View Journal | View Issue

Cite this: *RSC Adv.*, 2023, **13**, 24565

Research progress of metal–organic framework-based material activation of persulfate to degrade organic pollutants in water

Ruiyang Wen, Guoliang Shen * and Linghui Meng

The rapid development of industry in recent years has led to the introduction of serious pollutants into water bodies, and there is an urgent need for efficient organic degradation technologies. At present, selective peroxynitrite (PS) oxidation (SR-AOPs) is an effective way to treat pollutants in water bodies, and it is necessary to select a suitable material for the activation of peroxynitrite. Metal–organic frameworks (MOFs), with their tunable structure, large specific surface area, and tunable ligand molecules exhibit excellent reactivity and catalytic performance in the activation of persulfate. With MOF-based materials for PS activation as a novel advanced oxidation technology, this study reviews MOFs and their composites and derived materials. The current research status of activated persulfate for the treatment of organic pollutants in water, the influence of different systems on the degradation performance are discussed, and the activation and degradation mechanisms are discussed; the problems of the above materials in the degradation of organic pollutants are summarized, and research directions based on the coupled activated persulfate system of MOF materials are proposed.

Received 27th June 2023
Accepted 31st July 2023

DOI: 10.1039/d3ra04296k

rsc.li/rsc-advances

1 Introduction

Persistent organic pollutants are widely present in the effluents of chemical, dyeing, pharmaceutical, and paper industries, which has become a major environmental pollution problem. Thus, there is an urgent need for economical and efficient technologies to control and reduce persistent organic pollutants.[1] At present, advanced oxidation techniques represented by Fenton oxidation, ozone oxidation, electrochemical oxidation, and photocatalytic oxidation are the main methods for organic wastewater treatment,[2–4] and all of the above mentioned methods achieve the effective degradation of organic matter in water by releasing strong oxidants into the system, such as hydroxyl radical ($\cdot OH$), superoxide radical ($\cdot O_2^-$), and singlet oxygen ($^1O_2$), but the efficiency of oxidation treatment is relatively low. In recent years, advanced oxidation technology based on the release of persulfate radicals ($\cdot SO_4^-$) from peroxynitrite (PS) has become an efficient technology for the treatment of organic pollutants in water, and the redox potential of $\cdot SO_4^-$ (E^0 = 2.5–3.1 V) is slightly higher than that of $\cdot OH$ (E^0 = 1.8–2.7 V) and is more adaptable to the acidity and alkalinity of wastewater. Therefore, PS is gradually used by researchers to remove organic pollutants from water.[5–7] In the PS treatment of organic wastewater, PS requires highly reactive oxide species (ROS) activation to generate reactive oxygen species for the oxidative degradation and mineralization of organic pollutants metal oxygen/sulfide, carbon-based materials, metal-nonmetal composites, and MOF-based materials are widely used to activate persulphate to generate reactive oxygen species. With continuous research, MOFs are widely used in the treatment, and Fig. 1 shows some breakthroughs in the application of MOFs in the environmental field.[8,9]

Among many activation materials, MOF-based materials are highly active in the activation of PS for the removal of organic pollutants such as antibiotics and dyes in water due to their unique structural characteristics. As shown in Fig. 2, this paper retrieved the number of relevant articles on the activation of PS by MOF-based materials based on the Web of Science, which have been increasing year by year, especially in the removal of organic matter and has received much attention. Based on this, the author reviews the relevant studies of MOFs in the field of activated PS for the removal of organic pollutants in water, aiming to provide a reference for the study of advanced oxidation systems based on PS for MOF-based materials.

This paper focuses on the original MOFs and their composites and derivatives that can be used in the SR-AOPs process and provides an in-depth discussion and summary. Firstly, the mechanism of peroxynitrite-activated PS and its treatment of organic pollutants is described; secondly, the applications of the above materials in the SR-AOPs process are summarized; finally, the problems of existing MOF-based materials for the treatment of organic pollutants in water are presented, and the future research directions of MOF-based materials in SR-AOPs are prospected.

School of Petrochemical Engineering, Shenyang University of Technology, Liaoyang, 111003, China. E-mail: shengl_shxy@sut.edu.cn

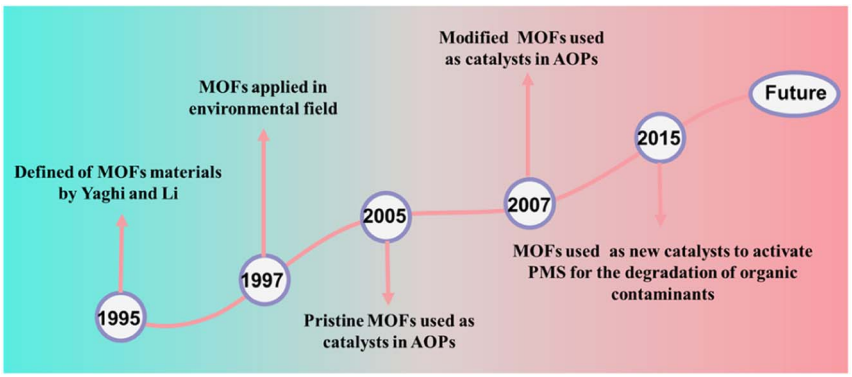

Fig. 1 Application of MOF materials in the field of environment.

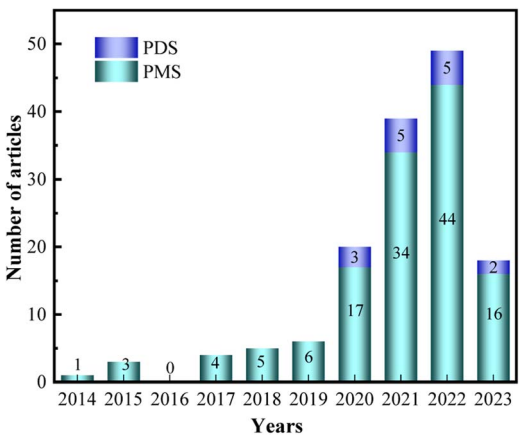

Fig. 2 The number of articles related to MOFs activating PS published in the recent 10 years (Source: Web of Science, Date: March 26, 2023, Keywords: MOF, PDS/PMS).

2 Activation mode and mechanism of persulfate

There are two types of PS used in the field of water pollution treatment, namely, peroxymonosulfate (PMS) and peroxydisulfate (PDS), both of which contain –O–O– bonds in their molecules and have the structures shown in Fig. 3. Peroxydisulfate has the advantages of single electron oxidation, low toxicity, low price, and simple operation; thus, it is widely used in the field of environmental treatment.

2.1 External energy activation PS mechanism

The efficiency of PS in the degradation system to produce ROS is a key factor in determining the efficiency of organic removal. To improve the efficiency of PS to produce ROS, it is often necessary to introduce some applied energy, and there are six main ways to activate PS with applied energy, namely, thermal activation, microwave activation, ultrasonic activation, optical activation, electrochemical activation, and plasma activation. Among them, thermal activation, electrical activation, and photoactivation of PS are more studied, and the rest of the activation methods are less studied.[10,11] The single applied energy activation of PS with single applied energy has the advantages of a simple process and no secondary pollution, but it causes a large amount of energy consumption such as electricity; thus, there is an urgent need to develop a low-cost activation method. As shown in Fig. 4, the activation mechanism is the same despite the different ways of applied energy, and the mechanism of various applied energy activation PS is to break the –O–O– bond in persulfate to produce $\cdot SO_4^-$ and ·OH to achieve the degradation of organic substances such as azo dyes and antibiotics.

2.2 Mechanism of PS activation by an external catalyst

2.2.1 Metal catalyst activation. In the degradation of pollutants such as organic dyes and drugs in water, ions or singlet catalytic activation of PS by transition metals such as Fe, Cu, Cr, Zn, Ag, and Co are commonly used to stimulate PS to produce $\cdot SO_4^-$ and ·OH radicals through the release of electrons from metal ions, which in turn removes molecules such as organic drugs and organic dyes. Among them, cobalt ion has the highest activation efficiency for PMS, while silver ion has the

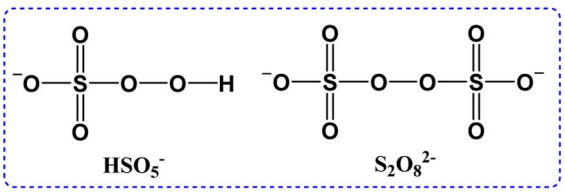

Fig. 3 Structure of persulfate.

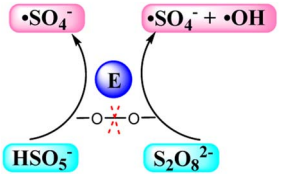

Fig. 4 Mechanism of activated persulfate.

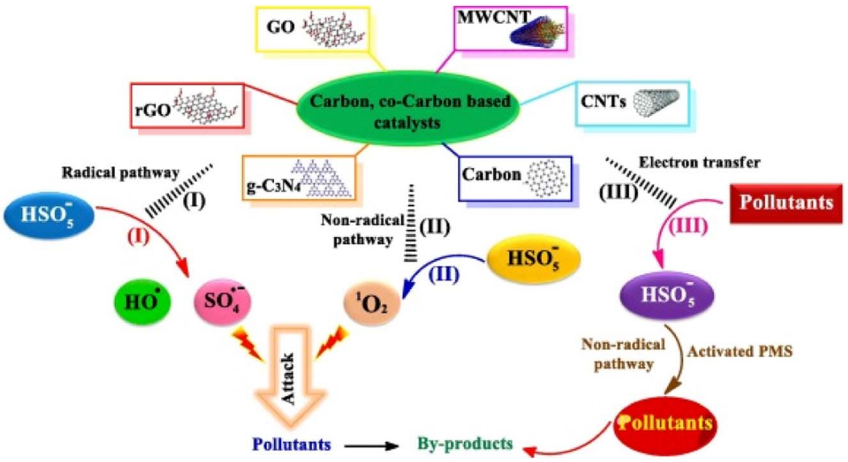

Fig. 5 The mechanism differences between traditional carbon and modified carbon materials in the activation of PMS.[16]

highest activation efficiency for PDS.[12] For example, the attack sites of $\cdot SO_4^-$ in Fe^0-activated PS for the degradation of sulfadiazine are usually S–C, S–N, and amino groups; multimetal catalysts activate PS mainly by the valence shift between metals and the valence shift between them and PS at the same time to achieve the degradation of organic drugs, and the co-activation in $NiCo_2O_4$-activated PS for the degradation of tetracycline is due to the valence shift between Ni^{3+}/Ni^{2+} and Co^{3+}/Co^{2+}.

The activation of PS by metal catalysts is certainly good, but the following issues need to be considered: (a) due to the cost of the metal itself, cheap and naturally abundant metals should be chosen as catalysts, such as Fe and Al. On the contrary, precious metals such as Ag are not suitable for industrial applications. In contrast, precious metals such as Ag are not suitable for industrial applications. (b) The compatibility of the metal itself with the environment, for example, the introduction of the heavy metals of Cu and Co, can lead to excessive heavy metals in living organisms. (c) Leaching loss of metal ions in solution.[13]

2.2.2 Material activation by MOFs. MOF-based materials with porous structures can be used as carriers for activating PS, and the rich metal centers of MOFs themselves provide active sites for activating PS. In 2015, Lin's group[14] first used MOFs as stand-alone catalysts for activating PS systems, and MIL-88A (Fe-MOF) was used as a stand-alone catalyst for activating PS to degrade organic dyes in water, opening up a new field of MOFs activation of PS systems.

For the first time, the group used MOFs as stand-alone catalysts for the activation of PS systems, and MIL-88A was used as a stand-alone catalyst for the activation of PS for the degradation of organic dyes in water, which opened up a new field of MOFs activation of PS systems. Subsequently, there have been numerous studies on the activation of PS systems based on MOF materials for the treatment of difficult to degrade organics in water, such as the treatment of organic dyes in water, endocrine disruptors in the environment, and antibiotics in water. Among them, there are three types of MOF-based material activation PS, which are single metal-based MOF material activation PS, MOFs doped with other materials to form composite materials such as X/Fe-MOF or X/Co-MOF activation PS, and X-MOF and other precursor-derived material activation PS. It is a promising treatment technology with the advantages of more active sites and higher degradation efficiency.

2.2.3 Carbon material PS activation mechanism. Carbon-based materials include traditional carbon materials (activated carbon, biochar, and semi-coke) and emerging carbon materials (graphene, carbon nanotubes, and Mxenes), which have the advantages of a cheap, energy-saving, nonpolluting, simple preparation process, and high catalytic activity, as shown in Fig. 5. Carbon in carbon-based materials mainly exists in the form of "π–π*", which plays the role of providing electrons during the activation of PS.[15] The four active sites of carbon surface functional groups, off-domain π-electrons, defect edge sp^2 hybridized carbon, and oxygen-containing functional groups need to be activated by contact with PS. The cost of PS activation by carbon-based materials is manageable, the preparation process is simple, and the sustained stability is good, but the activation efficiency of carbon-based materials is low compared to metals, and they are easily oxidized and difficult to recover.

3 Degradation mechanism of organic pollutants in SR-AOPs

The mechanisms of organic pollutant degradation by the currently proposed SR-AOPs technology can be summarized into two types of free radical mechanisms ($\cdot SO_4^-$, $\cdot OH$, and $\cdot O_2^-$) and non-free radical mechanisms (singlet oxygen $^1O_2$, electron transfer mechanism, high-valent metal oxidation mechanism), as shown in Fig. 6. The catalytic degradation of MOFs, MOFs composites, and MOF-derived metal oxides are mainly controlled by $\cdot SO_4^-$, while MOF-derived metal/carbon hybrids and carbon materials are controlled by nonradical-controlled pathways.[17,18] The advantages of a free-radical mechanism are high oxidation capacity and high mineralization rate but poor selectivity and few regenerable active sites. The advantages of a nonradical mechanism are high selectivity,

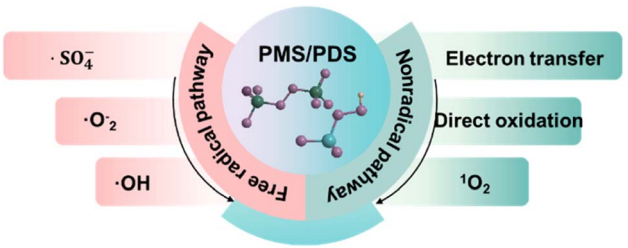

Fig. 6 Schematic diagram for activating PMS/PDS through two pathways.

high oxidation efficiency, and low system interference, but low mineralization rate and slow degradation rate. Therefore, the advantages of both mechanisms can be used to select the optimal treatment method for organic wastewater.

3.1 Free radical mechanism

For the free radical mechanism, the MOF material catalysts provide metal ions to participate in the redox reaction, and the metal ions activate PS to release $\cdot SO_4^-$ and $\cdot OH$ which have nonselective oxidative properties and are suitable for degrading organic pollutants in water with extremely strong oxidation potential. Through the free radical burst experiment, it can be found that $\cdot SO_4^-$ plays a dominant role in the degradation process, but can only mineralize organic pollutants into CO_2 and H_2O.

3.2 Non-free radical mechanisms

3.2.1 Single line state oxygen mechanism. In 1938, Kautsky[19] first described the process of oxygen formation in the excited form of $^1O_2$ by energy transfer, which has high reactivity for organic molecules rich in electrons (olefins, dienes, and polycyclic aromatic compounds), while if the target contains electron-absorbing groups, $^1O_2$ reacts with them at a reduced rate and exhibits a lower oxidation efficiency. Singlet oxygen is commonly found in photocatalytic reactions and is mainly involved in two electron reactions rather than free radical reactions.

3.2.2 Electron transfer mechanism. Electron transfer in non-free radical oxidation refers to the degradation of the target organism by providing electrons to the PS, with the catalyst in the system acting as an electron transfer medium or forming a complex with the oxidant PS to capture electrons from the organism. Electron transfer itself is a class of redox reactions, broadly divided into external electron transfer and internal electron transfer. In the outer mechanism, the ligand layer inside the metal ion does not move, there is no metal–ligand bond breakage and formation, and only a simple electron jump occurs. In the inner mechanism, there is a bridging ligand (Cl, OH, OH, NH, *etc.*) that connects the two metal ions and provides continuous coverage of orbitals for electron transfer. In organic chemistry, nonbonding and bonding are used to represent outer and inner electron transfer, respectively.

3.2.3 High-value metal oxidation mechanism. In metal-catalyzed activated PS systems, the presence of high-valent state metal intermediates, such as high-valent Fe, Mn, Cu, Ag, and Co, has been demonstrated. During their removal of organic matter, the physiological effect of the metal catalysts themselves to the environment should be considered. Whether the high-valence state metals are directly involved in the oxidation of the target pollutants or in other electron transfer processes is not yet clear; thus, the role of high-valence state metals in multiphase PS systems still awaits further attention from researchers.

4 MOFs activate PS to degrade organic pollutants

4.1 Fe-MOF-based catalysts

Fe-MOF catalysts for the degradation of organic pollutants by activated PDS mainly include MIL-88A (Fe), MIL-88B (Fe), MIL-101 (Fe), MIL-53 (Fe), and MIL-100 (Fe), which are widely used for the degradation of rhodamine B (RhB), acid orange (AO7), and orange-yellow G (OG), all of which are free radical degradation mechanisms.

Li[20] prepared a series of iron-based metal–organic frameworks such as MIL-101(Fe), MIL-100(Fe), MIL-5(Fe), and MIL-88B(Fe) by the hydrothermal method and investigated the catalytic performance of the above materials as catalysts to activate PDS for the degradation of AO7. The degradation process is a free radical mechanism, and the active species are $\cdot SO_4^-$ and $\cdot OH$. The magnitude of the ability of the above materials to degrade AO7 is known to be MIL-101(Fe) > MIL-100(Fe) > MIL-53(Fe) > MIL-88(Fe) by comparison, which is closely related to the metal ion activity of the catalyst itself and different cage sizes. The 95% degradation efficiency of AO7 was achieved in 2 h at AO7 = 80 mg L^{-1}, MIL-101(Fe) = 200 mg L^{-1}, PDS = 15 mM, initial pH = 6.16, T = 25 °C.

Mei[21] investigated the catalytic performance of MIL-53(Fe) activated PMS for the degradation of RhB with RhB = 40 mg L^{-1}, MIL-53(Fe) = 200 mg L^{-1}, PMS = 0.6 mM, initial pH = 5.0, and room temperature of 25 °C. The degradation efficiency of 100% was achieved in only 20 min. In the degradation process, $\cdot SO_4^-$ played a dominant role.

4.2 Co-MOF-based catalysts

Lin[22] reported that ZIF-67 activated PMS-degraded RhB and achieved 90% catalytic efficiency in only 60 min at RhB = 50 mg L^{-1}, ZIF-67 = 50 mg L^{-1}, PMS = 150 mg L^{-1}, and 20 °C, and the catalyst could be recycled with stable catalytic activity.

Wang[23] prepared a new Co-MOF micron sheet (BUC-92) and investigated the performance of BUC-92 activated PMS for the degradation of RhB, which had good stability and catalytic activity in the pH range of 3.0–9.0, and 10 mL RhB solution could be 100% degraded in only 1 min. To better evaluate the potential application value of BUC-92, the author simulated and constructed a fixed bed reactor. It is clear from the experimental results that $^1O_2$ plays an important role in the oxidation process. Lin[24] prepared $Co_3[Co(CN)_6]_2$ and similarly investigated the degradation ability of RhB with RhB = 10 mg L^{-1}, $Co_3[Co(CN)_6]_2$ = 50 mg L^{-1}, PMS = 50 mg L^{-1}, T = 30 °C, and the degradation

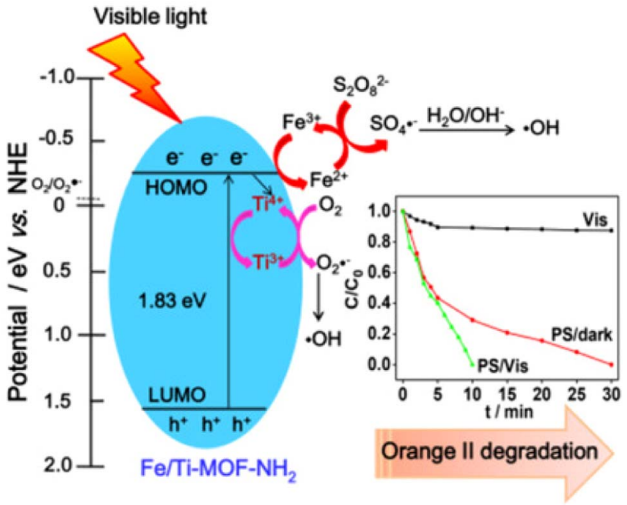

Fig. 7 Ti-MOF-based catalyst activates PDS to degrade Orange II.[25]

of RhB can be achieved to 100% in only 20 min. It can be seen that Co-MOF has excellent activity for activating PS.

4.3 Ti-MOF-based catalysts

Ti-MOF-based catalysts are more commonly used in photocatalysis but less commonly used in PS activation for organic wastewater treatment, Wang[25] prepared Fe/Ti-MOF-NH_2 by the solvothermal method and activated PDS to support visible light generation of $\cdot SO_4^-$ and $\cdot OH$ to catalyze the degradation of Orange II, at Orange II = 50 mg L^{-1}, Fe/Ti-MOF-NH_2 = 100 mg L^{-1}, PDS = 14 mM, initial solution pH = 5.0, T = 25 °C, and 100% degradation efficiency in only 10 min. The accelerated photocatalytic degradation of Orange II was attributed to the Fe^{3+}/Fe^{2+} and Ti^{4+}/Ti^{3+} redox cycles to promote electron transfer, and the introduction of PS effectively separated the photoexcited electron–hole to generate active the material catalyst to attack the N=N within the Orange II molecule, thus achieving the mineralized degradation of Orange II, as shown in Fig. 7.

In summary, Table 1 summarizes the related reports on the degradation of organic pollutants by MOF materials-activated PS, among which Fe-MOF and Co-MOF are reported more, while Cr is not common in the treatment of organic wastewater by activated PS because of its physiological influence on the environment.

5 Activation of PS by MOFs composites to degrade organic pollutants

The activation of PS by single MOF material often suffers from low catalyst activity and low pollutant removal efficiency, while the MOFs composite system can effectively solve this problem.

5.1 Co-MOF composite catalyst

In 2013, Hou[38] reported the pioneering work of native Co-MOF as a novel catalyst for organic pollutant degradation in SR-AOPS and explored the degradation experiments of Congo red dye using sodium persulfate as an oxidant. Among them, ZIF-67, a classical cobalt-based metal–organic framework material with the advantages of abundant active sites, high porosity, and stability in activated PS, is rapidly developing in the field of application for SR-AOPs. Azhar[34] synthesized highly stable bio-MOF-11 activated PS with submicron size to achieve sulfamoyl chloropyrazine (SCP) and *p*-hydroxybenzoic acid (*p*-HBA) at 25 °C, PMS = 500 mg L^{-1}, bio-MOF-11 = 50 mg L^{-1}, and an initial concentration of 45 mg L^{-1} of organic matter for only 5 min, and the activity of the catalyst did not decrease after recovery by water washing. The efficient degradation of bio-MOF-11 realized the application of MOF-based materials in the degradation

Table 1 The relevant reports on pristine MOF materials as catalysts for SR-AOPs

MOFs	Pollutant type and concentration	Oxidizer type and concentration	Reaction temperature and catalyst dosage	Degradation efficiency	Ref.
MIL-88A(Fe)	RhB, 10 mg L^{-1}	PDS, 200 mg L^{-1}	40 °C, 500 mg L^{-1}	80% (120 min)	14
ZIF-67	RhB, 50 mg L^{-1}	PMS, 150 mg L^{-1}	25 °C, 300 mg L^{-1}	90% (60 min)	26
$Co_3(BTC)_2$	DBP, 0.018 mM	PMS, 1.62 mM	25 °C, 300 mg L^{-1}	100% (30 min)	27
$Co_3[Co(CN)_6]_2$	RhB, 10 mg L^{-1}	PMS, 50 mg L^{-1}	30 °C, 50 mg L^{-1}	100% (20 min)	24
MIL-101(Fe)	AO7, 80 mg L^{-1}	PDS, 15 mM	25 °C, 200 mg L^{-1}	95% (120 min)	28
MIL-53(Fe)	AO7, 80 mg L^{-1}	PDS, 15 mM	25 °C, 200 mg L^{-1}	65% (120 min)	28
MIL-53(Fe)	AO7, 0.05 mM	PDS, 2 mM	25 °C, 600 mg L^{-1}	100% (90 min)	29
MIL-53(Fe)	OG, 0.2 mM	PDS, 32 mM	25 °C, 1 g L^{-1}	98% (120 min)	30
MIL-53(Fe)	OG, 0.2 mM	PDS, 32 mM	25 °C, 1 g L^{-1}	100% (90 min)	31
MIL-53(Fe)	RhB, 40 mg L^{-1}	PMS, 0.6 mM	25 °C, 200 mg L^{-1}	100% (20 min)	32
MIL-88A(Fe)	OG, 0.1 mM	PDS, 6 mM	25 °C, 300 mg L^{-1}	96% (120 min)	28
MIL-88B(Fe)	AO7, 80 mg L^{-1}	PDS, 15 mM	25 °C, 200 mg L^{-1}	25% (120 min)	28
Fe/Ti-MOF-NH_2	Orange II, 50 mg L^{-1}	PDS, 14 mM	25 °C, 100 mg L^{-1}	100% (10 min)	33
Bio-MOF-11-Co	Sulfachloropyradazine (SCP), 45 mg L^{-1}	PMS, 500 mg L^{-1}	25 °C, 50 mg L^{-1}	100% (15 min)	34
NH_2-MIL-101(Fe)	Amaranth(AMR), 50 mg L^{-1}	PMS, 200 mg L^{-1}	40 °C, 100 mg L^{-1}	100% (30 min)	35
NH_2-MIL-101(Fe)	BPA, 60 mg L^{-1}	PDS, 10 mM	25 °C, 200 mg L^{-1}	98% (120 min)	36
MIL-101(Cr)	Sulfonamide antibiotics(SMZ), 10 mg L^{-1}	PDS, 10 mM	25 °C, 150 mg L^{-1}	80% (90 min)	37

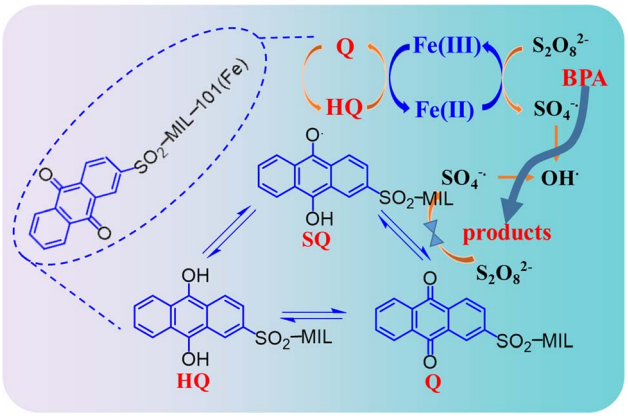

Fig. 8 Mechanism of BPA degradation catalyzed by AQS-NH-MIL-101(Fe).[36]

of pharmaceutical and personal care products in wastewater treatment.

5.2 Fe-MOF composite catalyst

Activation of PS by MIL-101(Fe) has been widely reported, and its framework with many metal active sites and stable structure is considered a widely used multiphase catalyst in the field of SR-AOPs. To improve the MIL-101(Fe)-catalyzed degradation process, it is necessary to increase its active sites to generate more radicals and thus improve the catalytic activity. The commonly used means are ligand introduction functional group modification, dopant modification, and energy introduction modification.

Li[36] prepared AQS-NH-MIL-101(Fe) by modifying NH_2-MIL-101(Fe) with 2-anthraquinone sulfonate (AQS) in Fig. 8; AQS can be used as a redox medium, thus activating PS to enhance the degradation of bisphenol A (BPA) with 97.7% removal rate, and the degradation of AQS-NH-MIL-101(Fe). The rate constant was 9 times higher than that of NH_2-MIL-101(Fe).

Activation time and temperature are important factors affecting the catalytic performance of MOFs. MIL-53(Fe) is the most studied pristine MOF among the SR-AOPs. Pu[31] investigated the catalytic performance of MIL-53(Fe) in the degradation of orange yellow G(OG) by activated PDS under different vacuum levels. It was found that the synthesis temperature can affect the crystallinity and catalytic activity of MIL-53(Fe), while the synthesis time can change the morphology of MIL-53(Fe) from collapsed octahedral to irregular morphology, thus changing the catalytic activity of MIL-53(Fe). The Fe^{II}-ligated and Fe^{III}-ligated unsaturated metal centers are catalytically active centers, and they can activate PDS to generate $\cdot SO_4^-$ or $S_2O_8^{\cdot-}$ to degrade OG.

5.3 Zr-MOF composite catalyst

The novel MOFs@COFs hybrid material UiO-66-NH_2@TpMA was first prepared by Lv[40] using a stepwise assembly method to activate PDS for the removal of bisphenol A (BPA), as shown in Fig. 9, under visible light at BPA = 50 mg L^{-1}, UiO-66-NH_2@-TpMA = 250 mg L^{-1}, PDS = 500 mg L^{-1}, pH = 5; the catalyst achieved 82% BPA degradation efficiency in 180 min and 69% degradation efficiency after 5 cycles, and the free radical scavenging experiments identified $\cdot SO_4^-$ as the main active substance in the oxidation process. The construction of MOFs@COFs hybrid materials expands the research ideas for MOF-based materials to activate PS, but the economic cost of COF materials is high and is not suitable for large-scale application.

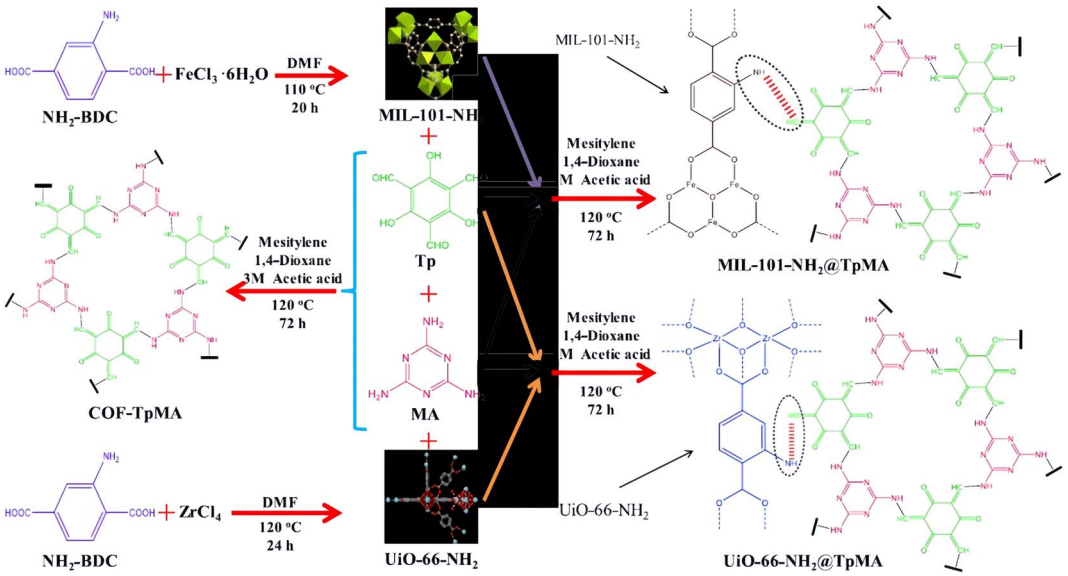

Fig. 9 The synthesis diagram of UiO-66-NH_2@TPMA.[40]

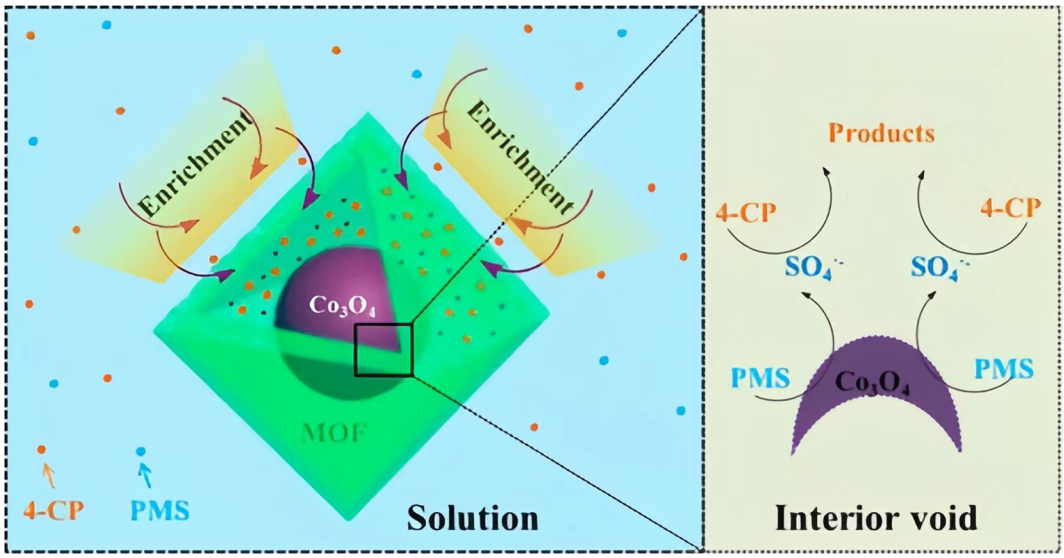

Fig. 10 The degradation mechanism of 4-CP by Co_3O_4@MOF-5.[41]

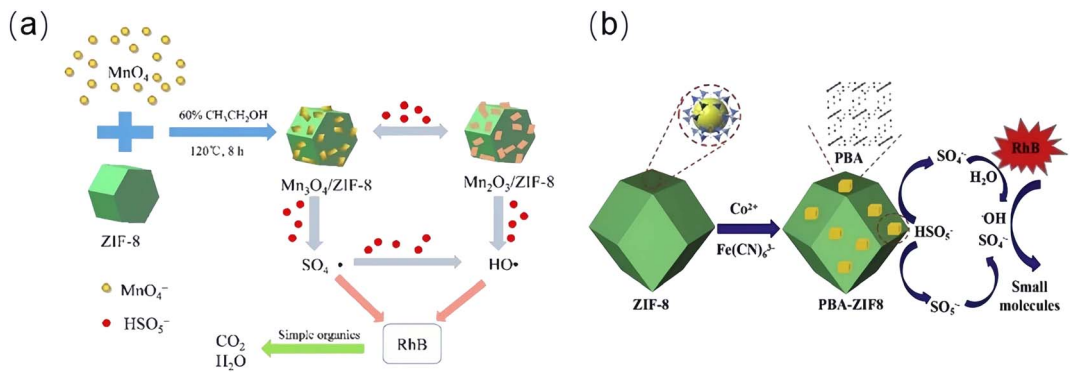

Fig. 11 Application of ZIF-8 composites in the degradation of RhB by activated PMS. (a) Mn_3O_4/ZIF-8 composite activated PMS for the degradation of RhB. (b) PBA-ZIF-8 composite activated PMS for RhB degradation.

5.4 Zn-MOF composite catalyst

Zeng[41] prepared a Co_3O_4@MOF-5 core–shell structured nanoreactor and successfully applied it to the degradation of the 4-chlorophenol (4-CP). It was found that the Co_3O_4@MOF-5 material with large nanopore size and open pore network (4 nm) enabled the rapid diffusion of PMS and 4-CP and products inside and outside the nanoreactor, providing a reaction site for the degradation of 4-CP (Fig. 10), Co_3O_4 and its surrounding voids enabled the rapid diffusion of 4-CP molecules into the active site of Co_3O_4, generating a large amount of $\cdot SO_4^-$, and 100% degradation of 4-CP could be achieved at a 4-CP solution concentration of 0.78 mM and a PMS concentration of 0.4 mM for 60 min. Thus, the degradation of 4-CP was enhanced. 99% 4-CP degradation efficiency could be achieved even after 4 cycles of Co_3O_4@MOF-5.

Hu[10] prepared Mn_3O_4/ZIF-8 composites by the hydrothermal method and used them to activate PMS for RhB degradation, as shown in Fig. 11a. The conversion between Mn_3O_4 and Mn_2O_3 can be realized by adding HSO_5^-. Mn_3O_4/Mn_2O_3 was uniformly distributed on the surface of ZIF-8. The Mn_3O_4/ZIF-8 composites had higher catalytic activity at a mass ratio of 1 : 2 of Mn_3O_4/ZIF-8, and the catalytic activity was higher at RhB = 10 mg L^{-1}, cat = 0.4 g L^{-1}, PMS = 0.3 g L^{-1}, T = 23 °C, the efficiency of RhB degradation reached 99.4% after 60 min. The ·OH was analyzed as a free radical involved in the degradation by the free radical burst experiment, and the degradation efficiency of 96% was still achieved after 5 cycles. On this basis, Ding[42] immobilized Prussian blue analogue (PBA) on ZIF-8 by the *in situ* growth method; the preparation of PBA-ZIF-8 and its degradation process of RhB are shown in Fig. 11b due to the addition of PBA, which greatly enhanced the catalytic efficiency during the degradation of RhB by activated PMS and only 30 min was needed to achieve the degradation efficiency of 97.5% at RhB = 20 mg L^{-1}, cat = 40 mg L^{-1}, PMS = 100 mg L^{-1}, and temperature of 25 °C. However, unlike Mn_3O_4/ZIF-8, it can be clearly seen that $\cdot SO_4^-$ played the role of the main free radical instead of ·OH in this experiment.

Table 2 Reports on MOFs composites as catalysts for SR-AOPs

MOFs	Pollutant type and concentration	Oxidizer type and concentration	Reaction temperature and catalyst dosage	Degradation efficiency	Ref.
PBA-ZIF-8	RhB, 20 mg L^{-1}	PMS, 100 mg L^{-1}	25 °C, 40 mg L^{-1}	97.5% (30 min)	42
$CoFe_2O_4$/ZIF-8	MB, 20 mg L^{-1}	PMS, 300 mg L^{-1}	20 °C, 50 mg L^{-1}	97.9% (60 min)	43
Mn_3O_4/ZIF-8	RhB, 20 mg L^{-1}	PMS, 300 mg L^{-1}	23 °C, 0.4 g L^{-1}	99.4% (60 min)	10
RGO/MIL-101(Fe)	Trichlorophenol (TCP), 20 mg L^{-1}	PDS, 20 mM	0.5 g L^{-1}	92% (180 min)	44
g-C_3N_4/MIL-101(Fe)	BPA, 10 mg L^{-1}	PDS, 1 mM	0.5 g L^{-1}	98% (60 min)	45
Co-MIL-101(Fe)	AO7, 0.1 mM	PDS, 8 mM	25 °C, 0.3 g L^{-1}	98% (150 min)	46
Cu-MIL-101(Fe)	AO7, 0.1 mM	PDS, 8 mM	25 °C, 0.3 g L^{-1}	92% (150 min)	46
Fe_3O_4@MOF-2	Diazinon, 30 mg L^{-1}	PDS, 10 mM	0.7 g L^{-1}	98% (120 min)	47
MIL-101-NH_2@TpMA	BPA, 50 mg L^{-1}	PDS, 500 mg L^{-1}	250 mg L^{-1}	99% (180 min)	40
UiO-66-NH_2@TpMA	BPA, 50 mg L^{-1}	PDS, 500 mg L^{-1}	250 mg L^{-1}	82% (180 min)	40

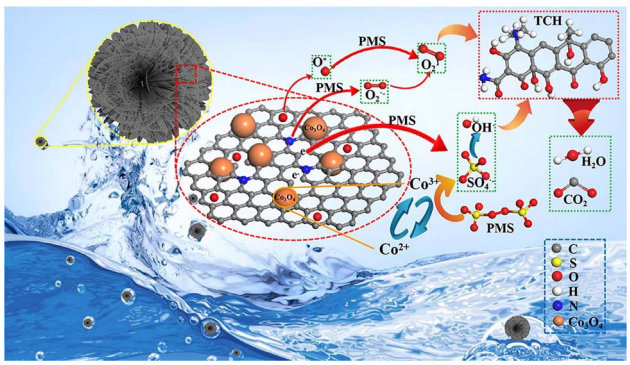

Fig. 12 Application of Co_3O_4/NC-activated PMS in the degradation of TCH.[48]

In summary, Table 2 summarizes the relevant reports of MOFs composites in activating PS to degrade organic pollutants. It is not difficult to see that the method of preparing MOFs composites is mainly to introduce oxides on the basis of the original MOFs to enhance their catalytic activity, and the oxides have good stability and will not affect the water itself.

6 MOF-derived activation of PS for the degradation of organic pollutants

The synthesis of MOF-derived materials is usually dependent on a specific gas atmosphere, such as N_2, Ar, or air. Through carbothermal reduction, metal ions surrounded by organic bonds in MOFs can be reduced to metal composites. Currently, in the process of activating PS, some MOFs with high nitrogen content (ZIF-8 and ZIF-67) can be directly carbonized at 600–1000 °C in the PS activation process to obtain nitrogen-doped porous carbon or nitrogen-doped metal oxides. It is important to develop a multi-stage high efficiency catalyst with multiple active sites to activate peroxymonosulfate (PMS) for the degradation of persistent organic pollutants. Wu[48] prepared cobalt oxide nanoparticles (Co_3O_4/NC) by pyrolysis using N–Co-MOF as the precursor, which showed excellent activity in activating PS for the removal of tetracycline hydrochloride (TCH), with a removal rate of 4.30% at 96 min under the combined action of $\cdot SO_4^-$ and $^1O_2$, and a kinetic constant 10.4 times higher than that of pure Co-MOF with the catalytic efficiency was significantly improved. Nitrogen-doped MOF-derived materials are the most commonly used to activate PMS, and most of the degradation processes are free radical degradation pathways; the flow of this experiment is shown in Fig. 12.

Table 3 Relevant reports on MOF-derived materials as catalysts for SR-AOPs

MOF-derived carbon materials catalyst name	Original MOFs	Pollutant type and concentration	Oxidizer type and concentration	Reaction temperature and catalyst dosage	Ref.
Fe@C-800	Fe-MOF	Sulfamethoxazole, 10 mg L^{-1}	PDS, 0.2 mM	30 °C, 0.4 g L^{-1}	39
N-doped porous carbon	ZIF-8	Phenol, 20 mg L^{-1}	PMS, 1.6 mM	25 °C, 200 mg L^{-1}	49
N-doped porous carbon	ZIF-8	*p*-Chloroaniline, 0.3 mM	PDS, 5 mM	25 °C, 150 mg L1	50
N-doped porous carbon	ZIF-8	RhB, 100 mg L^{-1}	PMS, 1.4 g L^{-1}	20 °C, 200 mg L^{-1}	51
N-doped porous carbon	Co–Fe PBAs	MB, 100 mg L^{-1}	PMS, 1 g L^{-1}	15 °C, 60 mg L^{-1}	52
N-doped porous carbon	Zn–Co PBAs	MB, 100 mg L^{-1}	PMS, 1 g L^{-1}	25 °C, 100 mg L^{-1}	53
N-doped graphene	MIL-100 (Fe)	Phenol, 50 mg L^{-1}	PMS, 3.25 mM	25 °C, 100 mg L^{-1}	54
N-doped graphene	MIL-100 (Fe)	*p*-HBA, 20 mg L^{-1}	PMS, 3.25 mM	25 °C, 100 mg L^{-1}	55
N, P, and S tri-doped hollow carbon shells	ZIF-67	BPA, 25 mg L^{-1}	PMS, 1.3 mM	20 °C, 60 mg L^{-1}	56
Nanoporous carbons	ZIF-8	Phenol, 20 mg L^{-1}	PMS, 1 g L^{-1}	25 °C, 0.1 g L^{-1}	57

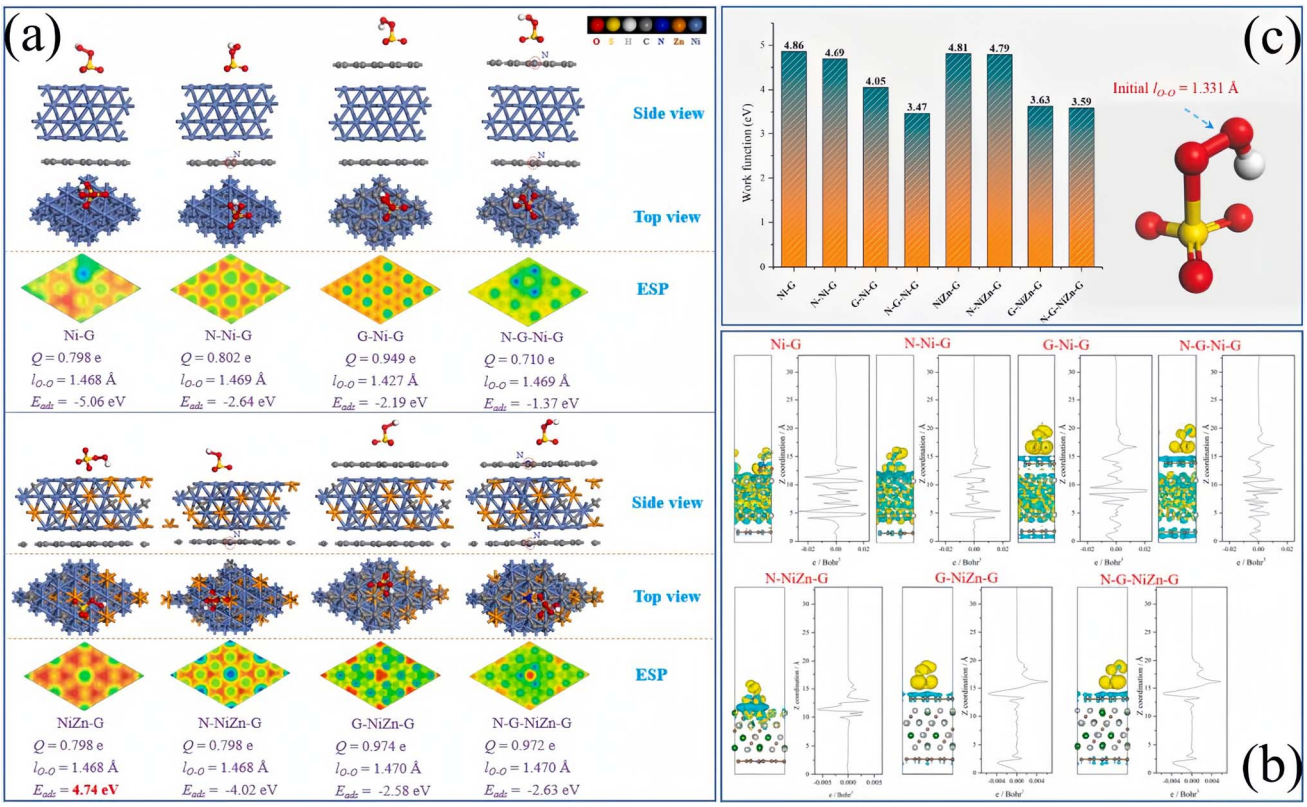

Fig. 13 (a) A series of results for DFT calculations, including adsorption models (top view, side view), electrostatic potential distributions (ESP, isosurface contour is 0.01 e per bohr^3), adsorption energy (E_{ads}), peroxide O–O bond length (l_{O-O}) and electron gain and loss of the adsorbed PMS (Q). (b) The charge difference distribution of different PMS adsorption models (isosurface contour is 0.002 e per bohr^3). The light green and light yellow denote the electron depletion and electron accumulation, respectively. (c) The work function (Φ) of each slab model.

In summary, Table 3 summarizes the application of MOF-derived materials in the degradation of organic pollutants by activated PS. The current research mainly uses MOFs as raw materials to prepare N-doped porous carbon by carbonization to realize the activation of PS.

7 DFT calculation for the activation of PS by MOFs

In the last decade, Density Functional Theory (DFT) calculations can probe the primitive steps and reaction mechanisms in multiphase catalytic processes at the atomic scale, providing important support for the development and application of catalytic materials. The DFT-based theoretical calculations are a powerful tool to predict and determine the possible degradation mechanisms and degradation pathways of SR-AOPs based on MOF materials and can simulate the energy changes in the reaction system at different stages. Among them, the adsorption energy E_{ads} is calculated as $E_{ads} = E_{total} - E_{catalyst} - E_{ps}$ (E_{total}, $E_{catalyst}$, and E_{ps} denote the adsorption on the PS catalyst surface, the electron transfer between the catalyst surface, and PS molecules between PS and MOFs, respectively). You[58] investigated the activation mechanism of PMS through the degradation of BPA in water by N-doped graphite-encapsulated NiZn@N-G-900-activated PMS obtained by MOF derivatization. The charge distribution on the catalyst surface was analyzed using electrostatic potential distribution (ESP) (Fig. 13a). The doping of graphite can effectively control the charge distribution on the catalyst surface and create more active sites. There is a strong interaction between the PMS and the catalyst (Fig. 13b), and the results of the charge difference distribution further verified that the PMS obtains electrons from the catalyst, and among the eight models established (Fig. 13c), the order of the work function is Ni-G (4.860 eV) > N-Ni-G (4.688 eV) > G-Ni-G (4.050 eV) > N-G-Ni-G (3.470 eV), (NiZn-G (4.799 eV) > N-NiZn-G (4.791 eV) > G-NiZn-G (3.634 eV) > N-G-NiZn-G (3.601 eV). The results show that both the graphite coating and the N-doped graphite coating can reduce the energy required for electrons to escape from the catalyst surface, thereby increasing charge transfer from the catalyst surface.

DFT calculation for predicting the chemical changes is an emerging research area, which still has some limitations and needs further in-depth study to better bridge the gap between theoretical calculations and experiments, and DFT+D and DFT+U (Hubbard U) calculation models are effective methods to solve the above problems.

8 Conclusion

MOF-based materials have great potential in the field of PS activation for the treatment of organic pollutants. The construction of MOFs composites and derivatives based on MOF materials can make MOF materials more durable, selective, or reactive in activated PS, or even provide additional functions for MOFs. The ROS of the measured reactions can be determined by radical trapping experiments, and thus the reaction pathways of the reactions can be determined. In SR-AOPs, DFT calculation plays a positive role; despite the limitations of DFT calculations, they can still provide some reference for predicting and determining the possible mechanisms and reaction pathways of MOF-based SR-AOPs.

In conclusion, the existing MOF-based materials can be both effective and stable catalysts in SR-AOPs but these materials still have some drawbacks in water treatment applications, including the loss of metal ions and certain problems in the subsequent separation of materials from solutions. For future research in the field of MOF-based SR-AOPs, the following aspects may need to be focused on.

(1) Preparation of stable MOF materials to avoid their metal precipitation in the process of use, resulting in metal ion pollution. Using MOF materials in the activation of PS to treat organic pollutants, the removal of pollutants is beneficial to the environment, but the decomposition of PS will continue to release elemental sulfur into the environment, and the impact of the release of elemental sulfur on the environment needs to be further investigated.

(2) Development of environment friendly, highly active, and low-cost MOF catalysts. Preparation of loaded MOFs catalysts based on MOF materials.

(3) In-depth exploration should be carried out to improve the recycling performance of MOF-based materials.

Author contributions

The main idea and framework of this paper were put forward by Guoliang Shen and Ruiyang Wen, and the manuscripts were written by Ruiyang Wen and Linghui Meng. The manuscripts were approved by all the authors.

Conflicts of interest

The authors declare that they have no conflicts of interest.

Acknowledgements

Thanks to all the authors for their efforts in completing this manuscript.

References

1 C. Li, B. Xu, L. Chen, M. Jin, G. Yi, L. Chen, B. Xing, Y. Zhang and Y. Wu, *Catal. Lett.*, 2022, DOI: **10.1007/s10562-022-04206-w**.
2 D. da Silva Bezerra, R. J. Franca and M. R. da Costa Marques, *Catal. Lett.*, 2021, **151**, 1477–1487.
3 A. Jawad, Z. Chen and G. Yin, *Chin. J. Catal.*, 2016, **37**, 810–825.
4 S. Yang, Y. Chen, H. Xu, P. Wang, Y. Liu and M. Wang, *Prog. Chem.*, 2008, **20**, 1433–1438.
5 J. Zhao, X. Duan and L. Guo, *Chin. J. Org. Chem.*, 2017, **37**, 2498–2511.
6 Y. Feng, Y. Li and G. Ying, *Prog. Chem.*, 2021, **33**, 2138–2149.
7 P. F. Xiao, L. An and D. D. Wu, *New Res. Carbon Mater.*, 2020, **35**, 667–681.
8 J. Liu, J. Shi, K. Fu, C. Ding, S. Gong and H. Deng, *Prog. Chem.*, 2021, **33**, 1311–1322.
9 X. Yang, S. Yang, X. Shao, L. Wang and R. Niu, *Prog. Chem.*, 2010, **22**, 2071–2078.
10 L. Hu, G. Deng, W. Lu, Y. Lu and Y. Zhang, *Chin. J. Catal.*, 2017, **38**, 1360–1372.
11 L. Xu, L. Qi, Y. Sun, H. Gong, Y. Chen, C. Pei and L. Gan, *Chin. J. Catal.*, 2020, **41**, 322–332.
12 G. P. Anipsitakis and D. D. Dionysiou, *Environ. Sci. Technol.*, 2004, **38**, 3705–3712.
13 W. Han and L. Dong, *Prog. Chem.*, 2021, **33**, 1426–1439.
14 K. Y. A. Lin, H. A. Chang and C. J. Hsu, *RSC Adv.*, 2015, **5**, 32520–32530.
15 X. Li, Z. Ye, S. Xie, Y. Wang, Y. Wang, Y. Lv and C. Lin, *Acta Chim. Sin.*, 2022, **80**, 1238–1249.
16 M. Kohantorabi, G. Moussavi and S. Giannakis, *Chem. Eng. J.*, 2021, **411**, 127957.
17 J. Scaria and P. V. Nidheesh, *Curr. Opin. Chem. Eng.*, 2022, **36**, 100830.
18 Y. Xu, T. Che, Y. Li, C. Fang, Z. Dai, H. Li, L. Xu and F. Hu, *Ecotoxicol. Environ. Saf.*, 2021, **223**, 112594.
19 H. Kautsky, *Trans. Faraday Soc.*, 1939, **35**, 216–219.
20 X. Li, W. Guo, Z. Liu, R. Wang and H. J. A. S. S. Liu, *Appl. Surf. Sci.*, 2016, **369**, 130–136.
21 W. Mei, D. Li, H. Xu, J. Zan, S. Lei, L. Qiang, B. Zhang, Y. Wang and D. J. C. P. L. Xia, *Chem. Phys. Lett.*, 2018, **706**, 694–701.
22 K. Y. A. Lin and H. A. Chang, *J. Taiwan Inst. Chem. Eng.*, 2015, **53**, 40–45.
23 F. X. Wang, Z. C. Zhang, X. H. Yi, C. C. Wang, P. Wang, C. Y. Wang and B. Yu, *CrystEngComm*, 2022, **24**, 5557–5561.
24 K. Y. A. Lin, B. J. Chen and C. K. Chen, *RSC Adv.*, 2016, **6**, 92923–92933.
25 M. Wang, L. Yang, C. Guo, X. Liu, L. He, Y. Song, Q. Zhang, X. Qu, H. Zhang, Z. Zhang and S. Fang, *ChemistrySelect*, 2018, **3**, 3664–3674.
26 J. Wang, J. Wan, Y. Ma, Y. Wang, M. Pu and Z. Guan, *RSC Adv.*, 2016, **6**, 112502–112511.
27 H. Li, J. Wan, Y. Ma, Y. Wang, X. Chen and Z. Guan, *J. Hazard. Mater.*, 2016, **318**, 154–163.
28 X. Li, W. Guo, Z. Liu, R. Wang and H. Liu, *Appl. Surf. Sci.*, 2016, **369**, 130–136.
29 Y. Gao, S. Li, Y. Li, L. Yao and H. Zhang, *Appl. Catal., B*, 2017, **202**, 165–174.
30 M. Pu, Y. Ma, J. Wan, Y. Wang, J. Wang and M. L. Brusseau, *Catal. Sci. Technol.*, 2017, **7**, 1129–1140.

31 M. Pu, Z. Guan, Y. Ma, J. Wan, Y. Wang, M. L. Brusseau and H. Chi, *Appl. Catal., A*, 2018, **549**, 82–92.
32 W. Mei, D. Li, H. Xu, J. Zan, L. Sun, Q. Li, B. Zhang, Y. Wang and D. Xia, *Chem. Phys. Lett.*, 2018, **706**, 694–701.
33 M. Wang, L. Yang, C. Guo, X. Liu, L. He, Y. Song, Q. Zhang, X. Qu, H. Zhang, Z. Zhang and S. Fang, *Chemistryselect*, 2018, **3**, 3664–3674.
34 M. R. Azhar, P. Vijay, M. O. Tade, H. Sun and S. Wang, *Chemosphere*, 2018, **196**, 105–114.
35 M. W. Zhang, K. Y. A. Lin, C. F. Huang and S. Tong, *Sep. Purif. Technol.*, 2019, **227**, 115632.
36 X. Li, W. Guo, Z. Liu, R. Wang and H. Liu, *J. Hazard. Mater.*, 2017, **324**, 665–672.
37 X. Huang, Q. Hu, L. Gao, Q. Hao, P. Wang and D. Qin, *RSC Adv.*, 2018, **8**, 27623–27630.
38 W. L. Hou, G. Y. Dong, Y. Q. Zhao and W. G. Zhang, *Synth. React. Inorg. Met.-Org. Chem.*, 2013, **43**, 1186–1189.
39 M. Pu, J. Wan, F. Zhang and M. L. Brusseau, *J. Hazard. Mater.*, 2021, **414**, 125598.
40 S. W. Lv, J. M. Liu, C. Y. Li, N. Zhao, Z. H. Wang and S. Wang, *Chemosphere*, 2020, **243**, 125378.
41 T. Zeng, X. Zhang, S. Wang, H. Niu and Y. Cai, *Environ. Sci. Technol.*, 2015, **49**, 2350–2357.
42 S. Ai, X. Guo, L. Zhao, D. Yang and H. Ding, *Colloids Surf., A*, 2019, **581**, 123796.
43 K. Zhang, D. Sun, C. Ma, G. Wang, X. Dong and X. Zhang, *Chemosphere*, 2020, **241**, 125021.
44 Y. Xu, Y. Wang, J. Wan and Y. Ma, *Chemosphere*, 2020, **240**, 124849.
45 Y. Gong, B. Yang, H. Zhang and X. Zhao, *J. Mater. Chem. A*, 2018, **6**, 23703–23711.
46 M. J. Duan, Zy. Guan, Y.-W. Ma, J. Q. Wan, Y. Wang and Y. F. Qu, *Chem. Pap.*, 2018, **72**, 235–250.
47 S. Sajjadi, A. Khataee, N. Bagheri, M. Kobya, A. Senocak, E. Demirbas and A. G. Karaoglu, *J. Ind. Eng. Chem.*, 2019, **77**, 280–290.
48 Q. Li, Z. Ren, Y. Liu, C. Zhang, J. Liu, R. Zhou, Y. Bu, F. Mao and H. Wu, *Chem. Eng. J.*, 2023, **452**, 139545.
49 G. Wang, S. Chen, X. Quan, H. Yu and Y. Zhang, *Carbon*, 2017, **115**, 730–739.
50 Y. Liu, W. Miao, X. Fang, Y. Tang, D. Wu and S. Mao, *Chem. Eng. J.*, 2020, **380**, 122584.
51 W. Ma, Y. Du, N. Wang and P. Miao, *Environ. Sci. Pollut. Res.*, 2017, **24**, 16276–16288.
52 N. Wang, W. Ma, Z. Ren, L. Zhang, R. Qiang, K. Y. A. Lin, P. Xu, Y. Du and X. Han, *Inorg. Chem. Front.*, 2018, **5**, 1849–1860.
53 N. Wang, W. Ma, Z. Ren, Y. Du, P. Xu and X. Han, *J. Mater. Chem. A*, 2018, **6**, 884–895.
54 P. Liang, C. Zhang, X. Duan, H. Sun, S. Liu, M. O. Tade and S. Wang, *Environ. Sci.: Nano*, 2017, **4**, 315–324.
55 P. Liang, C. Zhang, X. Duan, H. Sun, S. Liu, M. O. Tade and S. Wang, *ACS Sustainable Chem. Eng.*, 2017, **5**, 2693–2701.
56 W. Ma, N. Wang, T. Tong, L. Zhang, K. Y. A. Lin, X. Han and Y. Du, *Carbon*, 2018, **137**, 291–303.
57 P. Liang, Q. Wang, J. Kang, W. Tian, H. Sun and S. Wang, *Chem. Eng. J.*, 2018, **351**, 641–649.
58 J. You, C. Zhang, Z. Wu, Z. Ao, W. Sun, Z. Xiong, S. Su, G. Yao and B. Lai, *Chem. Eng. J.*, 2021, **415**, 128890.